PHYSICAL REVIEW C VOLUME 44, NUMBER 2 AUGUST 1991

Radial characteristics for nuclear states with weakly bound nucleons

W. Iskra
Soltan Institute for Nuclear Studies, Hoża 69, 00-681 Warsaw, Poland

I. Rotter
Zentralinstitut für Kernforschung Rossendorf, 0-8051 Dresden, Germany
(Received 28 January 1991)

The dipole transition densities as well as the radial pattern of partial widths for bound states embedded in the continuum, which are excited in the photonuclear reaction processes $^{16}O(\gamma,n)$ and $^{16}O(\gamma,p)$, are investigated in the framework of the continuum shell model for radii up to 11 fm. The $d_{3/2}$ nucleons in the resonance states of ^{16}O are loosely bound. Their extension well beyond the nuclear surface is taken into account in a straightforward manner. The interaction of the incoming photon with the nucleons of the target nucleus takes place mainly in the surface region at about 3 fm. The surface character is caused, above all, by geometrical effects. The nucleons emitted originate mainly from the interior of the nucleus due to the strong correlations of the nucleons. By this, the shell-model approach is justified in spite of the large radial extension of the $d_{3/2}$ nucleons.

I. INTRODUCTION

Recently, neutron-rich nuclei on the very edge of particle stability are studied experimentally in reactions induced by different incident particles [1,2]. Theoretically, the study of these nuclei is of interest because their properties are determined mainly by weakly bound neutrons which extend well beyond the nuclear surface. Bertsch and Esbensen [3] treated the nucleus as a three-body system consisting of two interacting nucleons together with a structureless core. They could reproduce the properties of ^{11}Li and ^{14}Be quite well. Hoshino *et al.* [4] performed large-scale shell-model calculations for light neutron-rich nuclei by taking into account the effect of loosely bound single-particle states. The radius of ^{11}Li came out close to the empirical value.

The theoretical problem of shell-model calculations for weakly bound states consists in the fact that the bound shell-model orbitals no longer provide a good starting point. When the residual interaction is neglected, some of the particles may even be unbound [3]. This problem raised for the description of the very neutron-rich nuclei exists, indeed, for all resonance states, also for those of stable nuclei. For example, even in such a stable nucleus as ^{16}O, the nucleons occupying the $1d_{3/2}$ shell in the interior are unbound if the residual interaction is not considered. In shell-model calculations this fact is ignored. All nucleons are considered to be bound. In the nuclear exterior the many-body effects are small. The correlations do not play a role and the interaction is close to the free-particle one. The $d_{3/2}$ particles are unbound. In order to describe the resonance states in a straightforward manner, one therefore has to include the unbound single-particle states from the very beginning in the calculations—not only for ^{11}Li but also for the resonance states of such a nucleus as ^{16}O.

In the continuum shell model [5], the Schrödinger equation is solved with bound and unbound single-particle states. Analytical formulas are given for the wave functions of the many-body states as well as some numerical results are obtained.

It is the aim of the present paper to discuss in detail the radial characteristics of a nuclear reaction induced by photons with emission of nucleons from resonance states to which the $d_{3/2}$ unbound states give an important contribution. While the photon interacts mainly at the surface of the nucleus, the nucleons are emitted in this reaction from the whole volume due to the correlations between the nucleons in the interior. This result justifies, on the one hand, the method to determine the spectroscopic properties of a nucleus by means of different nuclear reactions. On the other hand, it shows the importance of the correlations in the interior of the nucleus and therefore justifies the standard shell-model approach even in the case if nucleons, which are very loosely bound, give an important contribution to the wave function of the many-body system.

In Sec. II, the model is sketched while details of the calculations are given in Sec. III. In Sec. IV, the results for the transition densities are represented and compared to those obtained in the standard shell-model description. Furthermore, the radial pattern of the photonuclear reaction process is defined and numerical results for the $^{16}O(\gamma,p)$ and $^{16}O(\gamma,n)$ reactions are shown. Some conclusions are drawn in Sec. V.

II. CONTINUUM SHELL MODEL (CSM) WITH RADIAL DEPENDENCE

The CSM is a nuclear structure model in which the coupling to the continuum of decay channels is taken into account in a straightforward manner. It starts from the conventional shell model (SM) with single-particle (s.p.) basic states defined in a Woods-Saxon potential. Next,

the continuum of unbound s.p. states defined in the same potential is included by means of a coupled-channel method. The CSM allows a unified description of the structural (shell-model) and dynamical (coupled-channel calculations) aspects.

The details of the model can be found in Refs. [5] and [6]. Here, only the main idea of the model and those formulas, which are needed for the inclusion of the radial dependence into the CSM are presented, especially for the case of the photonuclear reactions.

The total functional space is subdivided, by using the projection operator technique, into the two orthogonal subspaces P and Q under the condition $P+Q=1$. The subspace Q contains the many-body states of A nucleons formed by the bound s.p. states and by the s.p. resonance wave functions up to some cutoff radius. Therefore, the structural part in the CSM is the same as in the standard SM approaches. The eigenstates Φ_R of the Q-projected Hamiltonian H_{QQ} are called [5] "quasibound stated embedded in the continuum" (QBSEC). These QBSEC's differ from the "bound states embedded in the continuum" introduced by Mahaux and Weidenmüller [7] by the contribution of the s.p. resonances from the interior of the nucleus. The subspace P contains the many-body states with $A-1$ nucleons in bound orbits and one nucleon in a scattering state as well as the part of the s.p. resonance wave functions beyond the cutoff radius.

When a nucleus is excited by an external electromagnetic field, the distortion of the nucleus is relatively small, and the process can be treated in a first-order Born approximation. In this case, the external field operator is not included into the nuclear Hamiltonian and the Schrödinger equation reads as follows:

$$(E-H)\Psi^F=F \ , \tag{2.1}$$

where F is the electromagnetic source term. In the photonuclear reactions, where the nucleus is excited by the interaction of the electromagnetic field H_{int} with the target nucleus in its ground state Φ_0, the source term reads

$$F=H_{int}\Phi_0 \ . \tag{2.2}$$

In such an approach, the F term contains the whole information on the dynamics of the photonuclear reaction. Hence, in order to study the radial dependence of the different characteristics of the photonuclear reactions in the entrance channel, the F term should be modified. In our opinion, the most natural and simple way is to change the source term as follows:

$$F\rightarrow F_{rr'}=F\delta(r-r')=H_{int}\delta(r-r')\Phi_0 \ , \tag{2.3}$$

where $\delta(r-r')$ is the Dirac delta function. Then, an integration over the radius variable r' in the matrix elements gives us the r-dependent characteristics.

Notice that we only use $\delta(r-r')$ instead of the full radial part of the Dirac delta function $\delta(r-r')/(rr')$ in order to keep the radial part of the spherical Jacobian r^2 in the radial integrals. The advantage of using (2.3) is that the contributions from different radial ranges to the total characteristics can be studied immediately. More precisely, if we consider, e.g., the cross section σ, our approach gives us the radial pattern of it, which is the contribution $\Delta\sigma(r_0)$ to the cross section σ from a small interval around r_0, including the geometrical effects. However, the total (integrated) physical cross section is not equal to the sum of the $\Delta\sigma(r_0)$ over all r_0 considered in the numerical integration because the interference effects arising from different radii are neglected. In this sense, the function $\delta(r-r')$ in (2.3) is dimensionless. The same is true for transition strengths also considered in the present paper.

In order to illustrate how this procedure works in practice, let us consider the transition from the ground state Φ_0 of the target nucleus A to the unbound state Ψ_E^c of the system $(A-1,1)$ under the electromagnetic perturbation H_{int}. Here the index c denotes a certain channel. In the first-order Born approximation, this process is described by the usual transition amplitude [8] $\langle\Psi_E^{c(-)}|F\rangle$, where $\Psi_E^{c(-)}$ is solution of the Schrödinger equation $(E-H)\Psi=0$ without source term. Now, in the radial-dependent case, we have the modified transition amplitude

$$W_r=\langle\Psi_E^{c(-)}|\delta(r-r')|F\rangle \ . \tag{2.4}$$

The solution Ψ_E^c of the Schrödinger equation reads

$$\Psi_E^c=\xi_E^c+\sum_R\tilde{\Omega}_R\frac{1}{E-\tilde{E}_R+i\tilde{\Gamma}_R/2}\langle\tilde{\Phi}_R^{(-)}|H|\xi_E^c\rangle \ , \tag{2.5}$$

where $\tilde{E}_R-i\tilde{\Gamma}_R/2$ are the complex eigenvalues of the energy-dependent effective Hamiltonian

$$H_{QQ}^{\text{eff}}=H_{QQ}+H_{QP}G_P^{(+)}H_{PQ} \tag{2.6}$$

in the Q subspace with coupling to the continuum. In (2.6) we use the standard notation $H_{QQ}=QHQ$, $H_{QP}=QHP$, etc., where Q and P denote the projection operators on the Q and P subspaces, respectively, G is the Green's function with appropriate boundary conditions, and G_P is its projection onto the subspace P. The eigenfunctions $\tilde{\Phi}_R$ of the effective Hamiltonian (2.6) include the effects of the external mixing due to the coupling to the continuum. In other words, $\tilde{\Phi}_R$ consists of different shell-model states Φ_R^{SM} mixed with different complex weights due to the nonvanishing second term in (2.6). The internal (configurational) mixing related to the pure structural shell-model Hamiltonian H_{QQ} is already contained in the functions Φ_R^{SM}.

The energy E_R and width Γ_R of a resonance state R are determined by solving the equations

$$E_R=\tilde{E}_R(E=E_R), \quad \Gamma_R=\tilde{\Gamma}_R(E=E_R) \ . \tag{2.7}$$

In the CSM, the function $\tilde{\Omega}_R$ in Eq. (2.5) is the wave function of the resonance state R,

$$\tilde{\Omega}_R(E_R)=\tilde{\Phi}_R(E_R)+\tilde{\omega}_R(E_R) \ , \tag{2.8}$$

where $\tilde{\omega}_R$, defined by

$$\tilde{\omega}_R=G_P^{(+)}H_{PQ}\tilde{\Phi}_R \ , \tag{2.9}$$

is the continuation of $\tilde{\Phi}_R$ into the continuum. By using the P projector,

$$P=\sum_c \int_{\varepsilon_c}^{\infty} dE|\xi_E^{c(+)}\rangle\langle\xi_E^{c(+)}|, \tag{2.10}$$

Eq. (2.8) reads as follows:

$$\tilde{\Omega}_R^{(+)}=\tilde{\Phi}_R^{(+)} + \sum_c \int_{\varepsilon_c}^{\infty} dE' \xi_{E'}^{c(+)} \frac{1}{E^{(+)}-E'} \times \langle \xi_{E'}^{c(+)}|H|\tilde{\Phi}_R^{(+)}\rangle , \tag{2.11}$$

where ε_c is the threshold energy of the channel c. Finally, the symbol ξ_E^c denotes the scattering wave function. It is solution of the P-projected Schrödinger equation in the coupled-channel representation

$$(E^{(+)}-H_{PP})\xi_E^{c(+)}=0 . \tag{2.12}$$

Coming back to the transition amplitude (2.4), it splits, according to (2.5), into three terms: (i) the direct term,

$$W_r^{(\mathrm{dir})}=\langle \xi_E^{c(-)}|\delta(r-r')|F\rangle , \tag{2.13}$$

(ii) the resonance term,

$$W_r^{(\mathrm{res})}=\sum_R \langle \tilde{\Phi}_R^{(-)}|\delta(r-r')|F\rangle \times \frac{1}{E-\tilde{E}_R+i\tilde{\Gamma}_R/2}\langle \tilde{\Phi}_R^{(-)}|H|\xi_E^{c(+)}\rangle , \tag{2.14}$$

and (iii) the channel-resonance scattering term (CHR),

$$W_r^{(\mathrm{CHR})}=\sum_R \langle \tilde{\omega}_R^{(-)}|\delta(r-r')|F\rangle \frac{1}{E-\tilde{E}_R+i\tilde{\Gamma}_R/2} \times \langle \tilde{\Phi}_R^{(-)}|H|\xi_E^{c(+)}\rangle . \tag{2.15}$$

In Eqs. (2.14) and (2.15), the matrix elements $\langle \tilde{\Phi}_R^{(-)}|H|\xi_E^{c(+)}\rangle$ are the amplitudes of the partial widths for the emission of nucleons from the excited resonance states R into the channels c.

In the following, we present the radial patterns of the photonuclear cross section, the corresponding dipole transition strengths and densities, as well as the amplitudes of the partial widths, which characterize the photonuclear process.

The cross section follows from the total wave function (2.5). It is the coherent sum of the direct, resonance, and channel-resonance terms in accordance with the three transition amplitudes (2.13)–(2.15). The direct reaction part of the cross section can be calculated by means of the scattering wave functions ξ_E^{cF} which obey the P-projected Schrödinger equation with source term

$$(E^{(+)}-H_{PP})\xi_E^{cF(+)}=PF\delta(r-r') . \tag{2.16}$$

The CHR scattering part follows from the coupled-channel wave functions defined by Eq. (2.9). According to (2.11), the $\tilde{\omega}_R$ do not depend on $F_{rr'}$. The resonance reaction part is connected with $\tilde{\Phi}_R$. It is the only part of the analog which is calculated in the usual SM.

To describe photonuclear reactions, the electric multipole strength of the resonance state R is defined [8] by

$$\tilde{D}_R(E_R)=CE_\gamma\langle \tilde{\Omega}_R||H_{int}||\Phi_0\rangle^2 . \tag{2.17}$$

Here, E_γ is the photon energy, C is a dimensionless constant, while the reduced matrix element $\langle \tilde{\Omega}_R||H_{int}||\Phi_0\rangle$ describes the transition from the target state Φ_0 to the resonance state $\tilde{\Omega}_R$ under the small distortion H_{int}. For electric dipole transitions, the space-dependent part of H_{int} reads rY_{1m} in the long-wavelength approximation. Defining

$$D_R=\tilde{D}_R(E=E_R) \tag{2.18}$$

in analogy to (2.7), one gets the following expression from (2.17) for the radial-dependent electric-dipole transition strength:

$$D_R=CE_\gamma\langle \tilde{\Omega}_R||rY_{1m}\delta(r-r')||\Phi_0\rangle^2 . \tag{2.19}$$

In the following, D_R is called the geometrical dipole transition strength. This expression is quadratic in the transition densities, both of which are taken at the same radius. That means interference effects from different radii are neglected. The dipole strengths are complex like the $\tilde{\Phi}_R$ and $\tilde{\Omega}_R$ due to the coupling of the resonance states to the continuum. They are directly connected with the resonance part of the photoabsorption cross section [8]

$$\sigma_\gamma^{\mathrm{tot}}(E)=\sigma_\gamma^{\mathrm{dir}}(E)-\mathrm{Im}\frac{1}{\pi}\sum_R \frac{\tilde{D}_R(E)}{E-\tilde{E}_R+i\tilde{\Gamma}_R/2} , \tag{2.20}$$

where $\sigma_\gamma^{\mathrm{dir}}$ denotes the direct part while the second term contains the resonance and channel-resonance parts of the total photonuclear reaction cross section.

III. DETAILS OF THE CALCULATIONS

In the present paper the $\gamma+{}^{16}\mathrm{O}$ reaction has been chosen to study the radial pattern of the photonuclear reactions. In the calculations, the four one-nucleon exit channels $(p+{}^{15}\mathrm{N}_{g.s.})$, $(p+{}^{15}\mathrm{N}^*)$, $(n+{}^{15}\mathrm{O}_{g.s.})$, and $(n+{}^{15}\mathrm{O}^*)$ with threshold energies taken from the experiment are considered. The wave functions of the target nuclei correspond to the $1p_{3/2}$ and $1p_{1/2}$ hole states of the ${}^{15}\mathrm{N}$ and ${}^{15}\mathrm{O}$ nuclei.

The shell-model calculations are performed using a Woods-Saxon potential for the single-particle states with parameters similarly to those in Ref. [9]. Also the Coulomb potential is included. The effective nucleon-nucleon forces are of the type

$$V(1,2)=-V_0(a+bP_{12}^\sigma)\delta(r_1-r_2) \tag{3.1}$$

with the parameters $V_0=500$ MeV fm^3, $a=1$, and $b=0.5$. The symbol P_{12}^σ denotes the spin-exchange operator.

In the compound nucleus ${}^{16}\mathrm{O}$, the resonance states with one-particle–one-hole (1p-1h) structure are considered, which are the dominating states excited in the $\gamma+{}^{16}\mathrm{O}$ reaction in the energy region of the giant dipole resonance. One of the nucleons is allowed to occupy the $(1d_{5/2}, 2s_{1/2}, 1d_{3/2})$ shells by leaving one hole in the $(1p_{3/2}, 1p_{1/2})$ shells. The $1d_{3/2}$ shells describe the part of the unbound $d_{3/2}$ orbits in the interior of the nucleus. Besides these 1p-1h states, more complicated ones with 2p-2h structure are considered. In these cases, two nu-

TABLE I. Shell-model energies E_R^{SM}, positions E_R, widths Γ_R, isospins T_R and leading configurations of the nine 1^- resonances with 1p-1h structure in ^{16}O.

State	Resonance R Leading configurations	T_R	E_R^{SM} (MeV)	E_R (MeV)	Γ_R (keV)
2	$2s_{1/2}1p_{1/2}^{-1}$	0	10.88	9.57	
3	$2s_{1/2}1p_{3/2}^{-1}$	1	13.59	13.22	230
4	$1d_{3/2}1p_{1/2}^{-1}$	0	16.79	16.85	600
5	$2s_{1/2}1p_{3/2}^{-1}$	0	16.91	15.96	520
6	$1d_{3/2}1p_{1/2}^{-1}$	1	17.57	17.35	310
7	$2s_{1/2}1p_{3/2}^{-1}$	1	20.11	19.61	140
8	$1d_{3/2}1p_{3/2}^{-1}$	0	22.49	22.44	480
9	$1d_{5/2}1p_{3/2}^{-1}$	1	23.92	22.45	1360
10	$1d_{3/2}1p_{3/2}^{-1}$	1	25.30	24.39	2000

cleons are allowed to occupy the ($1d_{5/2}$, $2s_{1/2}$, $1d_{3/2}$) shells by leaving two holes in the ($1s$) and ($1p_{3/2}$, $1p_{1/2}$) shells. The cutoff radius taken in the calculations is 7.5 fm. In the ^{16}O target ground state, all nucleons occupy the s.p. states up to the Fermi surface, i.e., the $1s_{1/2}$, $1p_{3/2}$, and $1p_{1/2}$ shells.

Diagonalizing the shell-model Hamiltonian H_{QQ}, 10 QBSEC's with 1p-1h structure and 76 with 2p-2h structure for $J^\pi=1^-$ are obtained. Every QBSEC contains, due to internal mixing, contributions from all states of the s.p. basis. The states with the largest weights are called leading configurations, although their weights are smaller than 0.7 in some cases.

Basing on these shell-model calculations, the coupled-channel equations are solved in the CSM in order to take into account the continuum influence including the "tails" of the $d_{3/2}$ unbound states. In this approach, all the parameters of the potential and the Hamiltonian are the same as in the shell-model calculations. Thus, a unified description of both the structure and the scattering characteristics is guaranteed.

Diagonalizing the effective Hamiltonian (2.6), one gets the resonance energies E_R (2.7) containing the effects of external mixing via the continuum of decay channels. Table I presents the shell-model energies E_R^{SM}, the CSM resonance energies E_R, widths Γ_R, isospins T_R, and the leading configurations for all 1p-1h 1^- QBSEC's. The leading configurations of the states 4, 6, 8, and 10 contain one particle in the $d_{3/2}$ shell which is, indeed, an unbound state. The isospin is not a good quantum number, but the impurities are small in most cases. Due to isospin mixing, D_R differs from zero for $T\approx 0$ states, but $|\mathrm{Re}D_R|$ is at least 2 orders of magnitude smaller than for $T\approx 1$ states [8]. The shifts $E_R - E_R^{SM}$ in the positions of the resonance states are caused by the coupling to the continuum. The two resonance states 8 and 9 with different isospin have different E_R^{SM} but almost the same E_R. The resonance state 1 is the center-of-mass spurious state. It is possible to exclude it by using the method given in Ref. [5]. Since, however, its mixing with the other resonance states is not significant in ^{16}O (see Ref [5]), we do not consider it in the following and do not exclude its small contributions to the physical resonance states.

The 1^- states with 2p-2h structure are described in

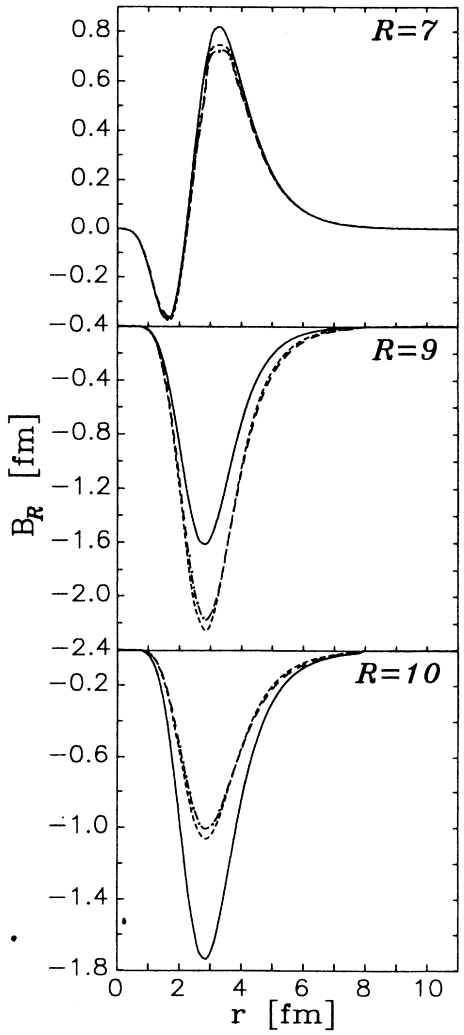

FIG. 1. The geometrical dipole transition densities for the resonance states 7, 9, and 10: B_R^{SM} (full line), B_R^{Φ} (dashed line), and B_R^{Ω} (dash-dotted line). The amplitudes B_R^{Φ} and B_R^{Ω} are calculated at the energies E_R.

Ref. [10]. Also, these states have contributions from configurations with particles in the $d_{3/2}$ unbound states.

IV. RADIAL PATTERN OF THE $\gamma + {}^{16}O$ REACTION

A. Dipole transition densities and partial widths

According to our approach, the radial profile of the transition strength (2.19) can be obtained for every QBSEC. First, let us consider the geometrical shell-model dipole transition densities

$$B_R^{\mathrm{SM}} = \langle \Phi_R || H_{int} \delta(r - r') || \Phi_0 \rangle \ . \tag{4.1}$$

They are real, energy independent, and play a basic role in the CSM since they are an input to the coupled-channel calculations. The full curves in Fig. 1 show the radial profile of the B_R^{SM} for the QBSEC's $R = 7, 9$ [giant dipole resonance, (GDR)], and 10 (see Table I). The states $R = 9$ and 10 have the leading configurations with one particle in a shell nlj with $n = 1$ while it is in a shell with $n = 2$ in the $R = 3$ and 7 cases. We see that the main contribution to the geometrical shell-model dipole transition density comes, in any case, from the ^{16}O surface region around 3 fm independent of the different nodes n in the leading configurations. By this the surface nature of the GDR is expressed.

The role of the continuum can be demonstrated from the analysis of the radial profiles of the following three geometrical dipole transition densities (GDTD): B_R^{SM},

$$\tilde{B}_R^{\Phi} = \mathrm{Re} \langle \tilde{\Phi}_R | \delta(r - r') | F \rangle \ , \tag{4.2}$$

$$\tilde{B}_R^{\Omega} = \mathrm{Re} \langle \tilde{\Omega}_R | \delta(r - r') | F \rangle \ . \tag{4.3}$$

They are displayed for $R = 7$, 9, and 10 in Fig. 1, too. One sees that the inner nuclear region ($r \leq 2$ fm) is almost not influenced by the continuum. The difference between $\tilde{B}_R^{\Phi}$ and $\tilde{B}_R^{\Omega}$ is small, even in the region of the nuclear surface. So, the wave function $\tilde{\omega}_R$ modifies the geometrical transition density only slightly and only in the surface region.

Calculations performed for the GDTD of the 2p-2h QBSEC's lead qualitatively to the same results. The surface character observed is therefore independent on the model space chosen.

Now let us examine the radial pattern of the partial width amplitudes

$$\chi_R^c = \langle \tilde{\Phi}_R^{(-)} | V \delta(r - r') | \xi_E^{c(+)} \rangle \ , \tag{4.4}$$

which give the contribution to the partial width amplitudes from a certain spatial region around r. In the following, χ_R^c will be called partial width profiles (PWP). They are, by definition, the exit channel analog of the GDTD (4.3). The PWP calculated for 27 resonance states with 2p-2h structure exhibit large contributions from the interior of the nucleus. A typical example is shown in Fig. 2. There is no surface effect due to the strong correlations between all the nucleons inside the nucleus, including the nucleons in the $d_{3/2}$ unbound states.

The many-particle wave function $\tilde{\omega}_R$ can be expanded in channel wave functions $\tilde{\omega}_R^c$ as follows:

$$\tilde{\omega}_R = A \sum_c | c \rangle \tilde{\omega}_R^c(r)/r \ . \tag{4.5}$$

Here, the symbol A represents the antisymmetrization operator. $\tilde{\omega}_R^c$ depend on the radial coordinate of one particle only [6] while $|c\rangle$ contains the dependence on spin, isospin, and angular coordinates of all particles as well as the radial coordinates of the $A - 1$ nucleons of the target. In Fig. 3, we see the radial dependence of $|\omega_R^c/r| = |\tilde{\omega}_R^c(E = E_R)/r|$ for the resonance $R = 9$ (and $c = 1$) for illustration. The main contribution to the matrix elements (4.3) arises from the region around 3 fm due to the radial part of the spherical Jacobian r^2 at small distances and due to the exponential decrease of the target wave function Φ_0 at large distances.

Next, let us consider the GDTD in detail. Recently, charge dipole transition densities (DTD) have been studied in the continuum random-phase-approximation (RPA) formalism [11]. Contrary to our approach, the

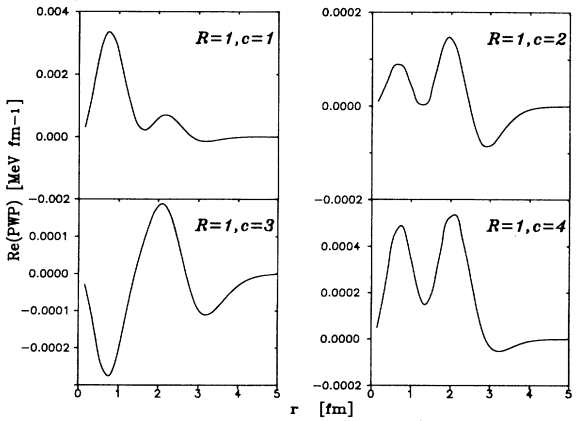

FIG. 2. The real parts of the PWP for one of the QBSEC's ($R = 1$), the wave function of which consists of large contributions from 2p-2h configurations and small ones from 1p-1h configurations; c denotes the number of the exit channel.

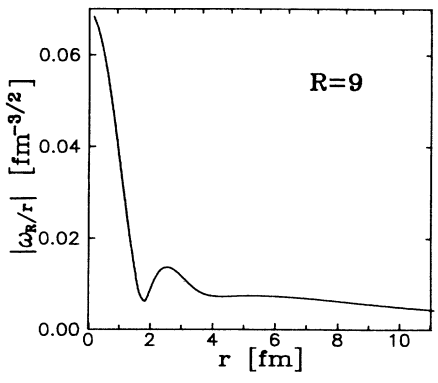

FIG. 3. The channel-resonance wave function $|\omega_R^c(r)/r|$ for the resonance 9 and the channel index $c = 1$ in dependence on the radius r. The wave function is calculated at the energy $E_{R=9}$.

DTD defined in Ref. [11] do not contain either the radial part of the dipole transition operator or the radial Jacobian r^2. In the RPA, the DTD are defined by means of the continuum excited-state wave function of a particular channel. This continuum wave function is the RPA analog to the CSM wave function Ψ_E^c. In the CSM, the GDTD is defined by means of the wave function $\tilde{\Omega}_R$ of the discrete state, in which the influence of all scattering channels is summed out. Just for that reason, the CSM GDTD is characteristic of the resonance state considered. The GDTD are defined in the CSM as in the common shell model, except that the continuum is treated rigorously. Consequently, the numerical results obtained for the GDTD in the CSM can be compared directly to the SM results, but not to the RPA ones.

Figure 4 shows the r dependence of the transition strengths D_R, Eq. (2.19), for four different resonances. The imaginary parts of the D_R of the two QBSEC's 3 and 7 are small in comparison with the corresponding real parts. This result is due to the fact that both resonances are well separated from other ones. The saddle structure obtained in the D_R of the $R=3$ and 7 states reflects the nodal shape of the $2s_{1/2}$ Woods-Saxon s.p. wave function, which contributes to the leading configuration of the collective states $R=3$ and 7. For the QBSEC 8, the imaginary part of D_R is relatively large. It results from the large external mixing between the two states of the resonance doublet $R=8$, 9. Here, the resonance state 9 is the giant resonance with $T\cong 1$ while the isospin of the other member of the doublet is $T\cong 0$. These two resonances overlap each other strongly and lose, as a matter of fact, their individuality.

B. Radial pattern of the cross section

While the cross section of the $\gamma+{}^{16}\mathrm{O}$ photonuclear reaction was calculated in many papers during the past years, the radial pattern of the cross section was not considered, up until now. The radial profile of the photonuclear reaction cross section is delivered by us, according to Sec. II, by neglecting the interference effects from different radii [see the remark below Eq. (2.19)]. The direct, channel-resonance, and full reaction cross sections are obtained in a wide region of the radius r where the interaction in the entrance channel takes place.

First, let us consider the behavior of the total cross section $\Delta\sigma$ as a function of the photon energy E_γ and the radius r, where the interaction of the incoming photon with the target nucleons takes place. The function $\Delta\sigma=\Delta\sigma(E_\gamma,r)$ is presented in Fig. 5. The GDR peak at $E_\gamma=22$ MeV has a maximum near $r=3$ fm. The saddle shape of the two peaks at $E_\gamma=13.2$ and 19.6 MeV in the r dependence reflects the $2s_{1/2}$ s.p. configuration with one node and two peaks in the leading configuration of the corresponding two QBSEC's $R=3$ and 7.

According to the splitting of the transition amplitude (2.4) into the three terms, (2.13)–(2.15), the full cross section can be divided into the direct, resonance, and channel-resonance parts. In Fig. 6, the radial profiles of the full, direct, and the sum of direct and CHR cross sections for every channel are considered at the photon energy $E_\gamma=22$ MeV. Here the resonance part, being of purely structural origin, is dominant. The $d_{3/2}$ unbound state is occupied in the leading configuration (see Table I). Only starting from very far distances, 8 fm, all three curves become of comparable magnitude. It is evident, however, that contributions from this far-space region to the total cross section can be neglected. In the region 2–4 fm, which contributes most strongly to the integrated total cross section, the role of the continuum is rather small. The oscillating character of the direct and CHR radial profiles results from the oscillating scattering wave functions which are solutions of the coupled-channel calculations. The analyzed example shows further that, in the GDR region, the inner nuclear region ($r<2$ fm) gives only a small contribution to the photodisintegration cross section. Some non-negligible contribution from the internal region arises only at $E_\gamma=19.6$ MeV from the first maximum of the saddle structure caused by the QBSEC 7.

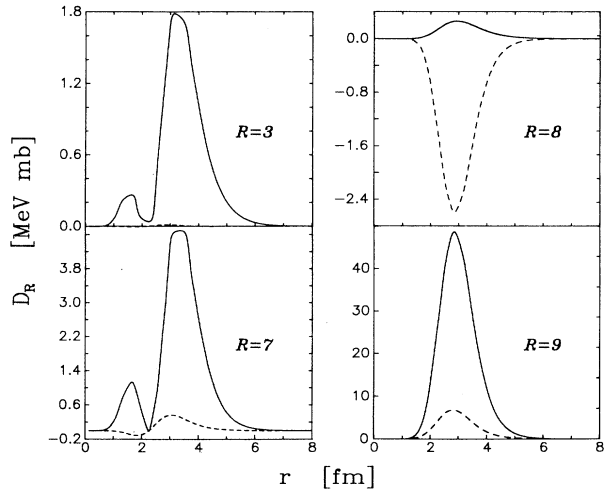

FIG. 4. The radial profiles of the geometrical dipole transition strengths for the resonance states $R=3$, 7, 8, and 9 at the energies of the corresponding resonances. The full lines correspond to $\mathrm{Re}(D_R)$ and the dashed ones to $\mathrm{Im}(D_R)$.

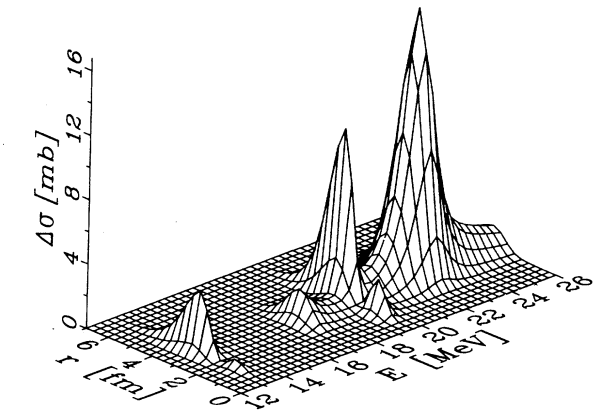

FIG. 5. The energy-radius three-dimensional plot of the total dipole photonuclear cross section of the $\gamma+{}^{16}\mathrm{O}$ reaction.

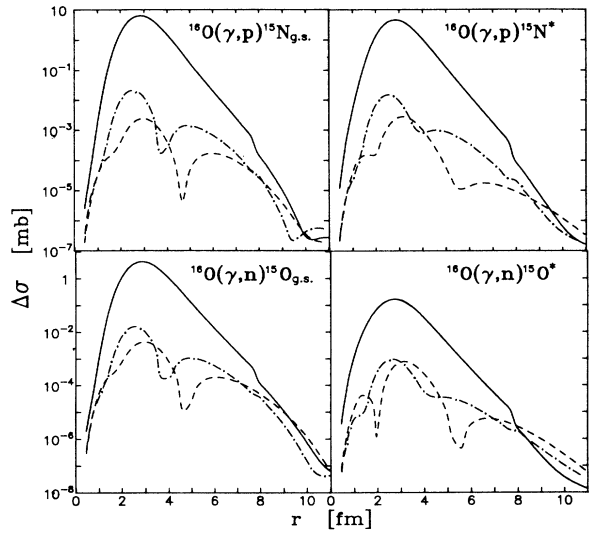

FIG. 6. The radial profiles of the cross section of the $^{16}O(\gamma,n)$ and $^{16}O(\gamma,p)$ reactions at the photon energy $E_\gamma = 22$ MeV. The full and dashed lines correspond to the full and direct fraction cross sections, respectively. The coherent sum of the direct and CHR cross sections is displayed by the dash-dotted line.

It is interesting to investigate the geometrical effects in the $\gamma + {}^{16}O$ reaction in more detail. In the present paper, the geometrical r^2 dependence of the GDTD is already taken into account in the definition (2.19) due to (2.3) [see the discussion below (2.3)]. Its influence is shown in Fig. 7. Here, the energy-radius contour map of the cross section is shown with F replaced by (2.3) as well as by

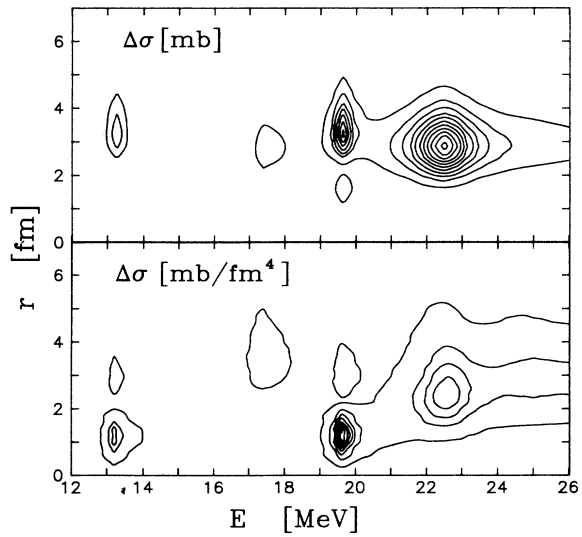

FIG. 7. The energy-radius contour map of the total dipole cross section of the $\gamma + {}^{16}O$ reaction with the source term (2.3) (upper part) and the source term (4.5) (lower part). The level interval is 1.5 mb (upper part) and 0.06 mb/fm^4 (lower part).

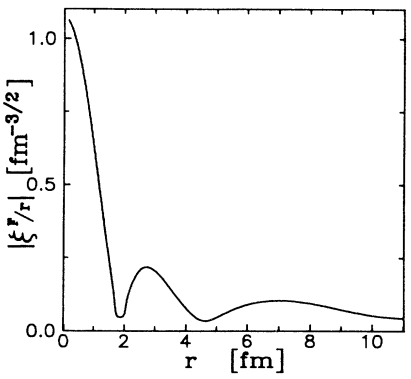

FIG. 8. The scattering wave function $|\xi^{cF}_E/r|$ vs radius for the channel index $c = 1$ at the photon energy $E_\gamma = 22$ MeV.

$$F \rightarrow \frac{F_{rr'}}{rr'} = \frac{F\delta(r-r')}{rr'} \quad . \tag{4.6}$$

As can be seen from the results, the surface character of the photonuclear reaction is mainly a geometrical effect above all in the regions at E_γ about 13 and 20 MeV. The direct reaction part also shows a maximum at about 3 fm as can be seen from Fig. 6 (dashed lines). This property results from the behavior of the scattering wave functions $|\xi^{cF}_E/r|$ (Fig. 8) which show the same behavior as the $|\omega^c_R/r|$ (see Fig. 3 and the following discussion). The influence of the interference effects from different radii is small, generally.

V. CONCLUSIONS

In this paper, the geometrical dipole transition densities, as well as the radial pattern of the partial widths and the profile of the photonuclear reaction cross sections on the double-magic nucleus ^{16}O are calculated by taking into account the coupling between bound and unbound states in a straightforward manner. The results obtained show that the interaction of the incoming particle with the target nucleus takes place in any case at the surface of the nucleus. The surface character is caused mainly by the geometrical factor arising from the spherical Jacobian r^2 in the radial integrals. The surface character is intensified by the factor $j_l(9r)$ (or r^l in long-wavelength approximation) in the integral describing the multipole transitions of the photonuclear reactions. Therefore, it will still be more marked in the higher multipole transitions than in the dipole transitions.

Based on these numerical results, we propose to include, at least, the geometrical factor from the Jacobian r^2 into the definition of the transition density. Otherwise, a radial dependence of the interaction between the incident particle and the nucleons of the nucleus is feigned which, in reality, does not exist. In the transition densities used in Ref. [11], these factors are not included. The authors mention, however, that the contributions of the p-h configurations which are dominant at low r are quenched in the integral, whereas those of the main p-h configurations at large r are enhanced. As a consequence,

the information on the microscopic structure of the state in the internal region is partially cut out. This statement corresponds exactly to the surface character of the photonuclear reactions observed in the present CSM calculations. Thus, the numerical calculations point to surface effects even in the light double-magic nucleus ^{16}O.

We conclude from our results that the "radius" of ^{16}O is about 3 fm in the photonuclear reaction. This value is in full agreement with the value of the rms for ^{16}O due to the realistic parameters used for the Woods-Saxon potential in our calculations. The results show further that the energy transferred to the nucleus in the photonuclear reaction is distributed over the whole nucleus, due to the strong correlations in the interior. The emission of the nucleons takes place, therefore, mostly from the internal part despite of the surface character of the photon-nucleus interaction.

The results obtained here show that the continuum shell model is a proper basis for describing the properties of nuclear states which consist of particles some of which are loosely bound and extended well beyond the nuclear surface. It is therefore suitable for a description of light neutron-rich nuclei.

ACKNOWLEDGMENTS

The authors are indebted to I. Turkiewicz for the suggestion to perform the present investigations. Valuable discussions with G.F. Bertsch are gratefully acknowledged.

[1] W. Mittig, J. M. Chouvel, Zhan Wen Long, L. Bianchi, A. Cunsolo, B. Fernandez, A. Foti, J. Gastebois, A. Gillibert, C. Gregoire, Y. Schutz, and C. Stephan, Phys. Rev. C **59**, 1889 (1987).

[2] I. Tanihata, T. Kobayashi, O. Yamakawa, S. Shimoura, H. Ekuni, K. Sugimoto, N. Takahashi, and T. Shimoda, Phys. Lett. B **206**, 592, (1988).

[3] G. F. Bertsch and H. Esbensen, Argonne National Laboratory Report No. PHY-6720-TH-90, 1990.

[4] T. Hoshino, H. Sagawa, and A. Arima, Nucl. Phys. **A506**, 271 (1990).

[5] H. W. Barz, I. Rotter, and J. Höhn, Nucl. Phys. **A275**, 111 (1977).

[6] I. Rotter, Fiz. Elem. Chastits At. Yadra **15**, 762 (1984) [Sov. J. Part. Nucl. **15**, 341 (1984)]; Rep. Prog. Phys. **54**, 635 (1991).

[7] C. Mahaux and H. A. Weidenmüller, *Shell Model Approach to Nuclear Reactions* (North-Holland, Amsterdam, 1969).

[8] I. Rotter, H. W. Barz, and J. Höhn, Nucl. Phys. **A297**, 237 (1978); J. Höhn, H. W. Barz, and I. Rotter, *ibid.* **A330**, 109 (1979).

[9] B. Buck and A. D. Hill, Nucl. Phys. **A95**, 271 (1967).

[10] P. Kleinwächter and I. Rotter, Phys. Rev. C **32**, 1742 (1985).

[11] M. Cavinato, M. Marangoni, and A. M. Saruis, Z. Phys. A **329**, 463 (1988); Nucl. Phys. **A496**, 108 (1989).